ARTICLE

Structural Evolution and Electronic Properties of $Au_2Ge_n^{-/0}$ (n=1−8) Clusters: Anion Photoelectron Spectroscopy and Theoretical Calculations†

Sheng-Jie Lu[a,b*], Umar Farooq[b,c], Hong-Guang Xu[b], Xi-Ling Xu[b], Wei-Jun Zheng[b,d*]

a. Department of Chemistry and Chemical Engineering, Heze University, Heze 274015, China
b. Beijing National Laboratory for Molecular Sciences, State Key Laboratory of Molecular Reaction Dynamics, Institute of Chemistry, Chinese Academy of Sciences, Beijing 100190, China
c. Department of Chemistry, COMSATS University Islamabad, Abbottabad-Campus, Pakistan
d. University of Chinese Academy of Sciences, Beijing 100049, China

(Dated: Received on February 27, 2019; Accepted on March 19, 2019)

Investigating the structures and properties of Au-Ge mixed clusters can give insight into the microscopic mechanisms in gold-catalyzed Ge films and can also provide valuable information for the production of germanium-based functional materials. In this work, size-selected anion photoelectron spectroscopy and theoretical calculations were used to explore the structural evolution and electronic properties of $Au_2Ge_n^{-/0}$ (n=1−8) clusters. It is found that the two Au atoms in $Au_2Ge_n^{-/0}$ (n=1−8) showed high coordination numbers and weak aurophilic interactions. The global minima of $Au_2Ge_n^-$ anions and Au_2Ge_n neutrals are in spin doublet and singlet states, respectively. $Au_2Ge_n^-$ anions and Au_2Ge_n neutrals showed similar structural features, except for $Au_2Ge_4^{-/0}$ and $Au_2Ge_5^{-/0}$. The C_{2v} symmetric V-shaped structure is observed for $Au_2Ge_1^{-/0}$, while $Au_2Ge_2^{-/0}$ has a C_{2v} symmetric dibridged structure. $Au_2Ge_3^{-/0}$ can be viewed as the two Au atoms attached to different Ge−Ge bonds of Ge_3 triangle. $Au_2Ge_4^-$ has two Au atoms edge-capping Ge_4 tetrahedron, while Au_2Ge_4 neutral adopts a C_{2v} symmetric double Au atoms face-capping Ge_4 rhombus. $Au_2Ge_{5-8}^{-/0}$ show triangular, tetragonal, and pentagonal prism-based geometries. Au_2Ge_6 adopts a C_{2v} symmetric tetragonal prism structure and exhibits σ plus π double bonding characters.

Key words: Photoelectron spectroscopy, Transition metal, Germanium cluster, Structural evolution, Quantum chemical calculations

I. INTRODUCTION

Germanium is extensively used in the fields of optoelectronics, bio-imaging, semiconductor materials, solar cells, polymerization catalyst, and field-effect transistors due to its excellent electron and hole mobilities [1–3]. Transition metal doped nanoclusters exhibit unique properties, such as quantum size effect, nonlinear optical effect, superparamagnetic relaxation, supersymmetry, and high catalytic performance remarkably different from bulk materials [4–6]. Pure germanium clusters have been extensively studied by various experimental techniques and theoretical calculations [7–18]. Recently, germanium clusters doped with transition metal have attracted great attention because they can form stable cage-like structures and induce novel magnetic properties (ferromagnetism, antiferromagnetism, and helimagnetism) [19–36]. These mixed clusters are potential building-blocks for manufacturing magnetoelectronics, magnetic memory devices, and skyrmion-based devices [37–45].

Gold has large electronegativity, high electron affinity, and strong relativistic effects [46, 47]. Especially, the strong relativistic effects can facilitate 6s-5d hybridization to induce various oxidation states [48, 49]. Under certain circumstances, an Au atom exhibits similar bonding properties to an H atom [50]. Therefore, these peculiar characteristics of gold may lead to the special growth patterns and unique electronic properties of Au-Ge mixed clusters. Gold doped germanium can be applied to produce infrared high-frequency photodetector because of its high charge carrier mobilities and long wavelength response [51]. Owing to the high thermoelectric power and hot electron effects, gold doped germanium films can be used for fabricating highly sensitive microsensors and cryogenic phonon sensors [52, 53]. The liquid phase soluble $[AuGe_{18}\{Si(SiMe_3)_3\}_6]^-$ and $[Au_3Ge_{18}]^{5-}$ clusters were synthesized and characterized previously [54, 55]. Recently, two-dimensional (2D) multi-phase germanene film was successfully synthesized by utilizing gold as a substrate [56]. Nevertheless, the catalytic mechanisms of 2D germanene film on the Au substrate re main un-

†Part of the special issue for "the 19th International Symposium on Small Particles and Inorganic Clusters"

*Authors to whom correspondence should be addressed. E-mail: lushengjie@iccas.ac.cn, zhengwj@iccas.ac.cn

clear. Investigating the structures and properties of Au-Ge mixed clusters, especially for multiple Au atoms doped germanium clusters may help to understand the microscopic mechanisms of gold-catalytic germanium films and to provide valuable information for developing germanium-based functional nanomaterials.

Previously, the structures, stabilities, and properties of germanium clusters doped with one or double Au atoms were studied by several theoretical calculations [57–62] and the photoelectron spectra of $AuGe_{1-12}^-$ were measured [63, 64]. But no experimental investigations of germanium clusters doped with double Au atoms have been reported in the literature. In order to gain more valuable information of Au−Ge mixed clusters, in this work, we investigated the structural evolution and electronic properties of $Au_2Ge_n^{-/0}$ (n=1−8) clusters using anion photoelectron spectroscopy and theoretical calculations. It is found that anionic and neutral Au_2Ge_{1-8} clusters show similar structural features and the two Au atoms have weak aurophilic interactions. Both anionic and neutral Au_2Ge_6 clusters have C_{2v} symmetric tetragonal prism structures and Au_2Ge_6 exhibits $\sigma+\pi$ double bonding characters.

II. EXPERIMENTAL AND THEORETICAL METHODS

Experiments were performed on an apparatus composed of a laser vaporization supersonic cluster source, a time-of-flight mass spectrometer, and a magnetic-bottle photoelectron spectrometer [65]. Briefly, the $Au_2Ge_n^-$ (n=1−8) clusters were produced in the laser vaporization source by focusing a pulsed laser beam (532 nm) from Nd:YAG laser (Continuum Surelite II-10) onto a rotating and translating Au/Ge mixture disk target (13 mm diameter, Au/Ge molar ratio 1/4). In the meantime, helium gas with ∼4 atm backing pressure was permitted to expand through a pulsed valve (General Valve Series 9) into the source to cool the formed $Au_2Ge_n^-$ clusters. The generated clusters were mass-analyzed with the time-of-flight mass spectrometer. The most abundant isotopologues of $Au_2Ge_{1-8}^-$ were selected with a mass gate, decelerated by a momentum decelerator, and then photodetached by laser beam (266 nm) from another Nd:YAG laser (Continuum Surelite II-10). The photodetached electrons were energy-analyzed by the magnetic-bottle photoelectron spectrometer to obtain the photoelectron spectra of $Au_2Ge_{1-8}^-$, which were calibrated with the spectra of Cu^- and Au^- taken at similar conditions. The resolution of the magnetic-bottle photoelectron spectrometer was approximately 40 meV at electron kinetic energy of 1 eV.

Theoretical calculations were performed using the Gaussian 09 program package [66]. The initial structures were obtained by putting the double Au atoms to different adsorption or substitution sites of the low-lying isomers of bare germanium clusters [7–16] and also by adding one Au atom to different adsorption of the low-lying isomers of $AuGe_n$ clusters [57–62]. Additionally, an unbiased search for the global minima of $Au_2Ge_{1-8}^-$ anions and their corresponding neutrals were also carried out using crystal structure analysis by particle swarm optimization (CALYPSO) software [67]. Details of CALYPSO software have been published elsewhere [68–74]. The Beck's three-parameter and Lee-Yang-Parr's gradient-corrected correlation hybrid functional (B3LYP) [75–78], Pople-type all-electron 6-31+G(d) basis set [79] for the Ge atoms, and the exchange-correlation potential and effective core pseudopotential LanL2DZ basis set [80] for the Au atoms were used in connection with the CALYPSO software. Full structural optimizations of $Au_2Ge_{1-8}^{-/0}$ clusters were performed employing density functional theory (DFT) in the context of B3LYP that is suitable for investigating TM-Ge mixed clusters [36, 63]. Pople-type all-electron 6-311+G(d,p) basis set [81] was used for the Ge atoms and the scalar relativistic effective core potential Stuttgart/Dresden(SDD) basis set [82] was used for the Au atoms. During the overall geometry optimizations for both anionic and neutral clusters, no symmetry constraint was used. To confirm that the obtained structures were true local minima on the potential energy surfaces, harmonic vibrational frequency analyses were employed. To further accurately evaluate the relative energies of isomers, the single-point energies of $Au_2Ge_{1-8}^{-/0}$ clusters were calculated by the coupled-cluster methods including single, double, and perturbative contributions of connected triple excitations (CCSD(T)) [83, 84] using the optimized geometries at the B3LYP level. The augmented correlation-consistent polarized valence triple-zeta (aug-cc-pVTZ-PP) [85] basis set and the augmented correlation-consistent polarized valence double-zeta (aug-cc-pVDZ-PP) [86] basis set were chosen for the Au and Ge atoms, respectively. Theoretical vertical detachment energies (VDEs) were calculated by the energy differences between the neutral and anionic states both using the anionic geometries, while theoretical adiabatic detachment energies (ADEs) were calculated by the energy differences between the neutral and anionic states using the respective optimized geometries. Zero-point energy (ZPE) corrections obtained from the B3LYP functional were considered in computing the relative energies and ADEs of isomers. Natural population analysis (NPA) was performed to explore the charge distributions of $Au_2Ge_{1-8}^-$ within the natural bond orbital (NBO) version 3.1 programs [87–94]. The Multiwfn program (3.41 package) [95] was used to analyze the orbital compositions of the most stable isomer of $Au_2Ge_6^-$ by natural atomic orbital (NAO) method. NAO method has much better basis set stability or insensitive and stronger theoretical basis than Mulliken or Mulliken-like methods, such as modified Mulliken population defined by Ros & Schuit (SCPA) [96, 97].

DOI:10.1063/1674-0068/cjcp1902036

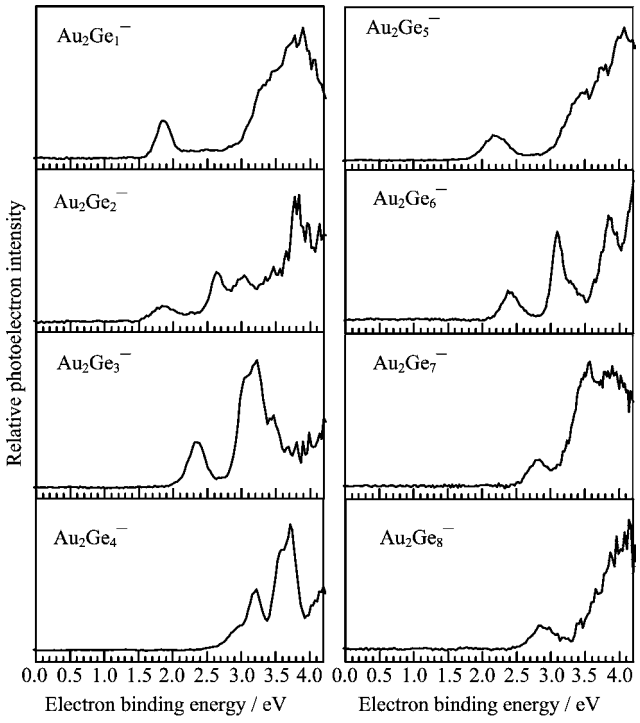

FIG. 1 Photoelectron spectra of $Au_2Ge_n^-$ (n=1−8) clusters recorded with 266 nm photons.

III. EXPERIMENTAL RESULTS

Photoelectron spectra of $Au_2Ge_{1-8}^-$ anions recorded with 266 nm photons are shown in FIG. 1. The experimentally measured VDEs and ADEs of $Au_2Ge_{1-8}^-$ are summarized in Table I. The VDE of each anion was determined by the maximum of the first peak in the photoelectron spectrum, whereas the ADE of each anion was obtained by adding the instrument resolution to the electron binding energy (EBE) values at the crossing point, in which a straight line was drawn along the leading edge of the first peak to cross with the baseline of spectrum.

As shown in FIG. 1, the spectrum of $Au_2Ge_1^-$ reveals a small peak centered at 1.85 eV, a shoulder peak centered at 3.43 eV, and a high-intensity broad peak centered at 3.89 eV. The spectrum of $Au_2Ge_2^-$ possesses three peaks centered at 1.87, 2.64, and 3.04 eV, respectively, and a barely resolved high-intensity broad peak at 3.81 eV. The spectrum of $Au_2Ge_3^-$ displays a peak centered at 2.35 eV, followed by a high-intensity broad peak centered at 3.22 eV, a shoulder peak centered at 3.47 eV, and some unresolved weak peaks beyond 3.60 eV. Similarly, the spectrum of $Au_2Ge_4^-$ shows a low-intensity shoulder peak at 2.96 eV, a major peak at 3.22 eV, a high-intensity peak at 3.72 eV, and a peak above 4.20 eV.

As for $Au_2Ge_5^-$, a low-intensity peak centered at 2.16 eV, followed by three high-intensity peaks centered at 3.46, 3.78, and 4.08 eV is observed. In the case of $Au_2Ge_6^-$, the spectrum shows a low-intensity peak centered at 2.38 eV, two high-intensity peaks centered at 3.10 and 3.85 eV, and a high-intensity peak beyond 4.20 eV. For the spectrum of $Au_2Ge_7^-$, a low-intensity peak centered at 2.82 eV and two roughly recognized high-intensity broad peaks centered at 3.57 and 3.90 eV, can be observed. A low-intensity peak centered at 2.85 eV, and some indiscernible high-intensity peaks

TABLE I Relative energies, theoretical VDEs and ADEs of the low-lying isomers of $Au_2Ge_n^-$ (n=1−8) clusters, along with the experimental VDEs and ADEs estimated from their photoelectron spectra.

Isomers		State	ΔE[a]	VDE/eV		ADE/eV	
				Theo.[b]	Expt.[c]	Theo.[b]	Expt.[c]
$Au_2Ge_1^-$	**1A**	$^2A''$	0.00	1.84	1.85	1.81	1.62
	1B	$^2\Pi$	0.72	2.63		2.55	
$Au_2Ge_2^-$	**2A**	$^2A_1$	0.00	1.81	1.87	1.49	1.39
	2B	$^2\Sigma$	0.25	3.80		3.62	
	2C	$^2B_{3g}$	0.55	2.38		1.00	
$Au_2Ge_3^-$	**3A**	^2A	0.00	2.37	2.35	2.04	2.09
	3B	$^2A'$	0.25	2.13		1.83	
	3C	^2A	0.28	2.24		1.93	
	3D	$^2A_1$	0.33	3.09		2.46	
$Au_2Ge_4^-$	**4A**	^2A	0.00	2.81	2.96	2.48	2.54
	4B	$^2B_2$	0.15	2.79		2.16	
	4C	^2A	0.34	2.16		2.02	
	4D	$^2A_1$	0.39	2.45		2.21	
$Au_2Ge_5^-$	**5A**	^2A	0.00	2.10	2.16	1.82	1.78
	5B	$^2A'$	0.07	3.53	3.47	2.81	2.90
	5C	$^2A'$	0.11	2.44		1.80	
	5D	^2A	0.14	2.36		1.87	
$Au_2Ge_6^-$	**6A**	$^2A_1$	0.00	2.26	2.38	2.14	2.10
	6B	^2A	0.15	2.26		2.04	
	6C	^2B_u	0.19	2.84		2.46	
	6D	$^2A'$	0.23	3.04		2.69	
$Au_2Ge_7^-$	**7A**	^2A	0.00	2.64	2.82	2.35	2.46
	7B	$^2B_1$	0.10	2.91		2.61	
	7C	^2A	0.30	2.55		2.39	
	7D	^2A	0.43	2.80		2.31	
$Au_2Ge_8^-$	**8A**	^2A	0.00	2.65	2.85	2.07	2.37
	8B	^2A	0.08	2.21		2.03	
	8C	^2A	0.10	2.69		2.45	
	8D	^2A	0.19	3.02		2.49	

Note: the isomers labeled in bold are the most probable isomers in the experiments.
[a] The ΔEs (in eV) values are calculated at CCSD(T)/aug-cc-pVTZ-PP/Au/aug-cc-pVDZ/Ge level.
[b] The ADEs and VDEs are calculated at B3LYP/SDD/Au/6-311+G(d,p)/Ge level.
[c] The uncertainties of the experimental VDEs and ADEs are ±0.08 eV.

DOI:10.1063/1674-0068/cjcp1902036

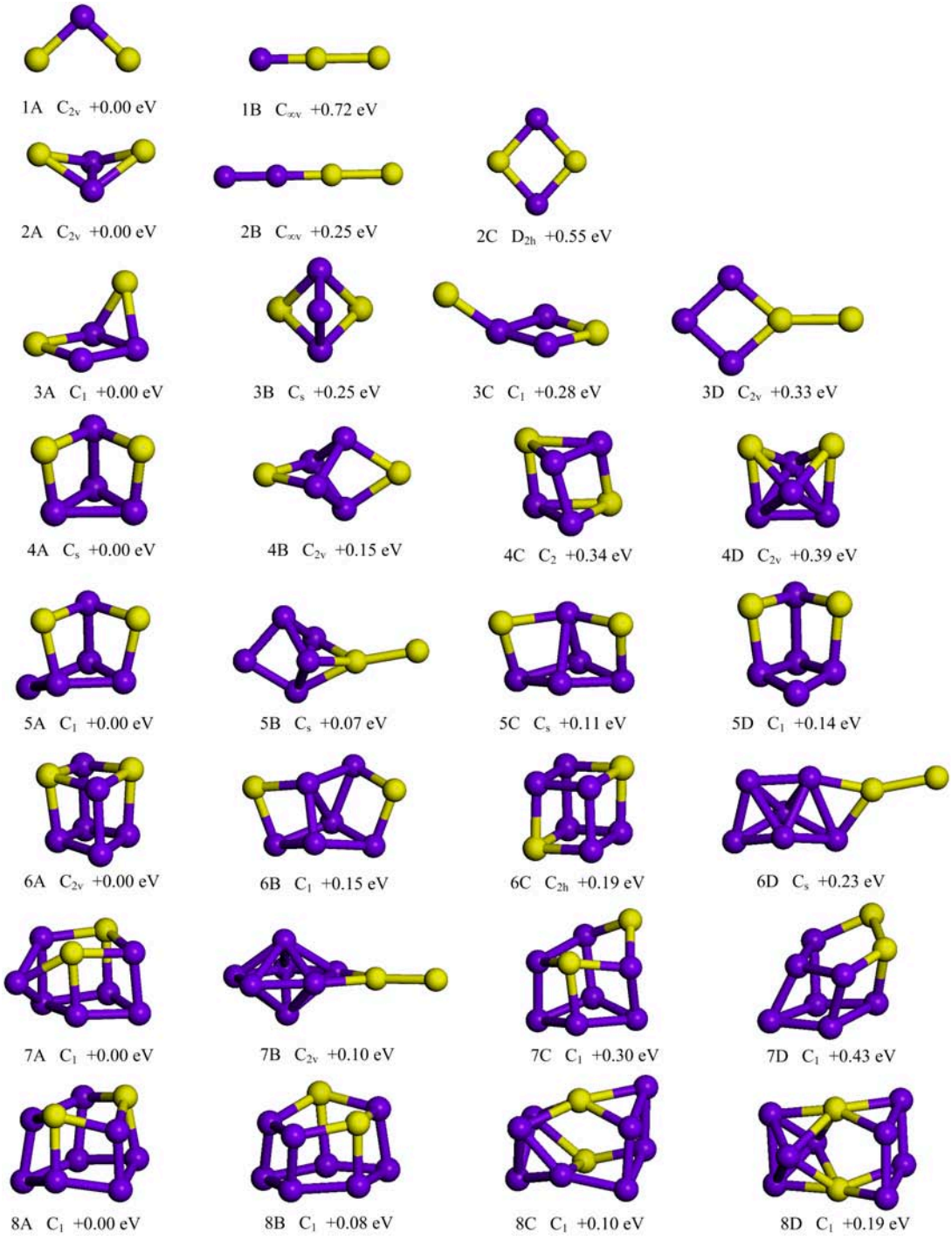

FIG. 2 Typical low-lying isomers of anionic $Au_2Ge_n^-$ (n=1−8) clusters. Yellow and purple balls stand for the Au atoms and Ge atoms, respectively. ΔE values are calculated at CCSD(T)/aug-cc-pVTZ-PP/Au/aug-cc-pVDZ/Ge level of theory.

between 3.30 and 4.20 eV, can be found in the spectrum of $Au_2Ge_8^-$.

IV. THEORETICAL RESULTS

The typical low-lying isomers of $Au_2Ge_{1-8}^-$ obtained at the B3LYP level are presented in FIG. 2. The relative energies (ΔE), theoretical VDEs and ADEs of these low-lying isomers are summarized in Table I, along with the experimental VDEs and ADEs. The bond lengths of the most stable isomers of $Au_2Ge_n^-$ (n=1−8) clusters are shown in Table II. According to the generalized Koopmans' Theorem (GKT) [98, 99] we simulated the photoelectron spectra of the low-lying isomers of

DOI:10.1063/1674-0068/cjcp1902036

TABLE II The bond lengths of the most stable isomers of $Au_2Ge_n^{-/0}$ (n=1−8) clusters.

Isomer[a]	Bond length/Å	Isomer[b]	Bond length/Å
1A	Au−Au=3.63	1A′	Au−Au=3.49
	Au−Ge=2.48		Au−Ge=2.42
2A	Au−Au=4.23	2A′	Au−Au=3.36
	Au−Ge=2.68		Au−Ge=2.63
	Ge−Ge=2.45		Ge−Ge=2.51
3A	Au−Au=4.18	3A′	Au−Au=3.56
	Au−Ge=2.55−2.80		Au−Ge=2.53−2.81
	Ge−Ge=2.48−2.52		Ge−Ge=2.55
4A	Au−Au=3.47	4A′	Au−Au=5.21
	Au−Ge=2.54−2.56		Au−Ge=2.62−2.63
	Ge−Ge=2.53−2.55		Ge−Ge=2.57
5A	Au−Au=3.70	5A′	Au−Au=3.37
	Au−Ge=2.53−2.58		Au−Ge=2.53−2.73
	Ge−Ge=2.52−2.60		Ge−Ge=2.50−2.60
6A	Au−Au=3.26	6A′	Au−Au=3.58
	Au−Ge=2.62−2.65		Au−Ge=2.56−2.62
	Ge−Ge=2.56−2.61		Ge−Ge=2.56−2.63
7A	Au−Au=3.21	7A′	Au−Au=3.27
	Au−Ge=2.59−2.72		Au−Ge=2.55−2.71
	Ge−Ge=2.55−2.78		Ge−Ge=2.47−2.63
8A	Au−Au=3.40	8A′	Au−Au=3.60
	Au−Ge=2.58−2.62		Au−Ge=2.54−2.68
	Ge−Ge=2.49−2.67		Ge−Ge=2.48−2.64

[a] The isomer of $Au_2Ge_n^-$(n=1−8).
[b] The isomer of Au_2Ge_n neutrals.

$Au_2Ge_{1-8}^-$ and named them as density of states (DOS) spectra similar to our previous reports [68–74, 100]. The comparison of the DOS spectra and experimental spectra is shown in FIG. 3.

A. $Au_2Ge_1^-$

In the global minimum (1A) of $Au_2Ge_1^-$, the two Au atoms bond with the Ge atom to form a C_{2v} symmetric V-shaped structure with a nonbonding Au−Au distance of 3.63 Å. The ∠AuGeAu angle in $Au_2Ge_1^-$ is calculated to be 94.0°. The theoretical VDE of isomer 1A (1.84 eV) is very close to the experimental value (1.85 eV) and its DOS spectrum can roughly reproduce the peak positions, patterns, and intensities of the experimental spectrum, although the higher electron binding energy (EBE) peaks in the DOS spectrum are slightly narrower than those in the experimental one. Isomer 1B is unlikely to exist in the molecular beams because it is less stable than isomer 1A by 0.72 eV. Thereby, we suggest that isomer 1A is the most probable structure observed in the experiments.

B. $Au_2Ge_2^-$

The most stable isomer (2A) of $Au_2Ge_2^-$ shows a C_{2v} symmetric bibridged structure and the distance between the two Au atoms is 4.23 Å. Isomer 2B is a $C_{\infty v}$ symmetric Ge−Ge−Au−Au linear structure. The theoretical VDE of isomer 2A (1.81 eV) agrees well with the experimental value (1.87 eV) and its DOS spectrum is also in reasonable agreement with the experimental spectrum, although the relatively spectral intensities are slightly different. Isomers 2B and 2C are higher in energy than isomer 2A by at least 0.25 eV. Thus, isomer 2A is suggested as the most probable one contributing to the photoelectron spectrum of $Au_2Ge_2^-$ and the contribution of isomers 2B and 2C to the experimental spectrum can be ruled out.

C. $Au_2Ge_3^-$

As for $Au_2Ge_3^-$, the most stable isomer (3A) can be described as an Au atom edge-capping a Ge−Ge bond of $AuGe_3$ rhombus with a nonbonding Au−Au distance of 4.18 Å. The theoretical VDE of isomer 3A (2.37 eV) gives good agreement with the experimental value (2.35 eV) and its DOS spectrum can fit the experimental spectrum well, except for the relatively spectral intensities. Isomers 3B, 3C and 3D are less stable than isomer 3A by at least 0.25 eV. Therefore, isomer 3A is suggested to be the most probable structure existing in the cluster beams.

D. $Au_2Ge_4^-$

In the lowest-lying isomer (4A) of $Au_2Ge_4^-$, the two Au atoms interact with the four Ge atoms to form a triangular prismatic structure with the distance of two Au atoms being 3.47 Å. The theoretical VDEs of isomer 4A (2.81 eV) and isomer 4B (2.79 eV) show reasonable agreement with the experimental value (2.96 eV). The DOS spectrum of isomer 4A can roughly reproduce the peak positions, patterns, and intensities of the experimental spectrum and that of isomer 4B also matches with the experimental peaks at 2.96, 3.22, and 3.72 eV. Isomer 4B is slightly higher in energy than isomer 4A by 0.15 eV. Isomers 4C and 4D being less stable than isomer 4A by at least 0.34 eV are unlikely to be detected in the experiments. Therefore, isomer 4A is suggested to be the most probable structure detected in the experiment and isomer 4B might have minor contribution to the experimental spectrum.

E. $Au_2Ge_5^-$

Isomers 5A and 5B are almost degenerate in energy. Isomer 5A adopts a Ge-capped Au_2Ge_4 triangular prismatic structure with the two Au atoms having a distance of 3.70 Å. Isomer 5A can be obtained by adding

DOI:10.1063/1674-0068/cjcp1902036

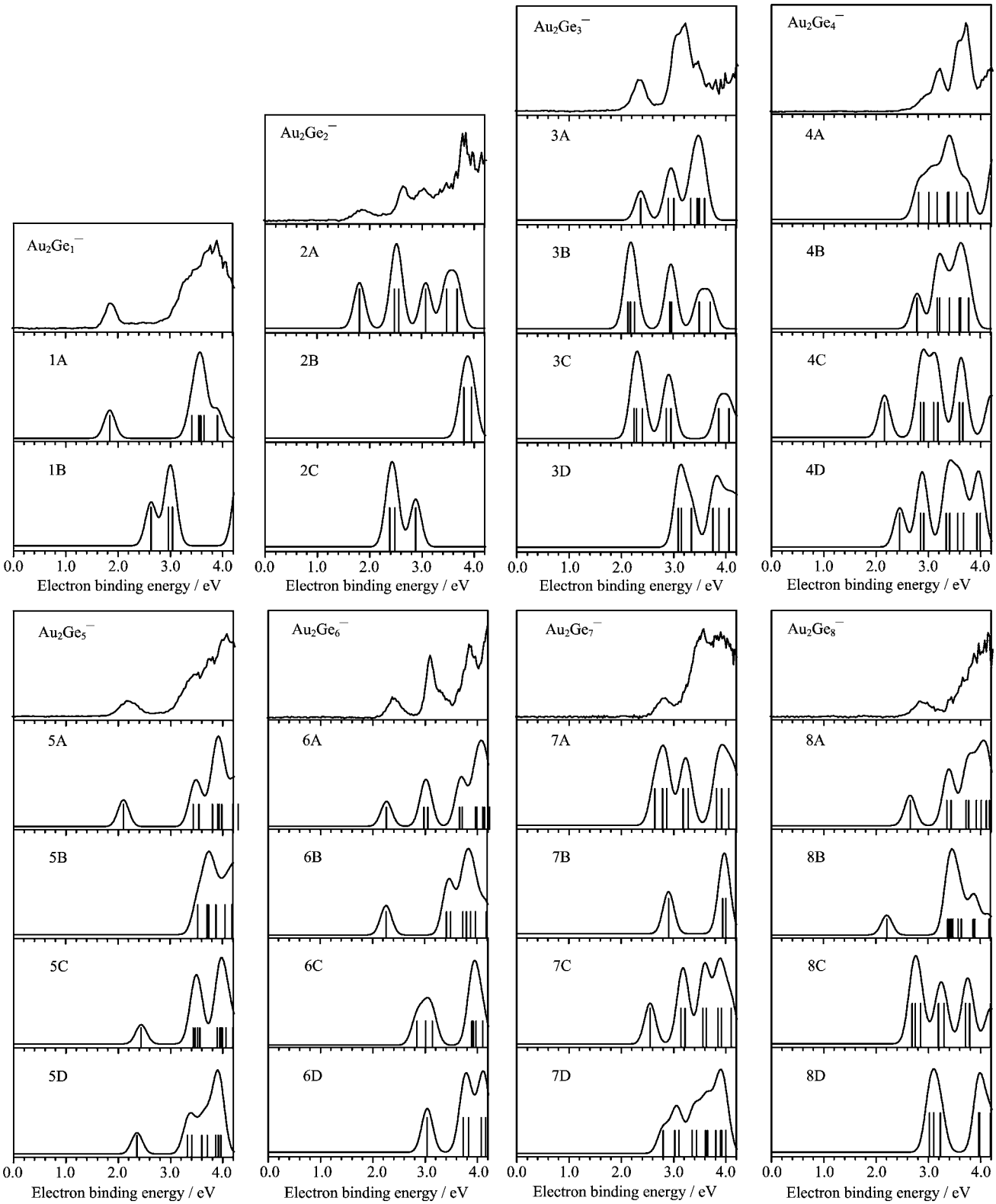

FIG. 3 Comparison between the experimental photoelectron spectra and simulated DOS spectra of the low-lying isomers of $Au_2Ge_n^-$ (n=1−8) clusters. Simulated spectra were obtained by fitting the distribution of the transition lines with the unit area Gaussian functions of 0.20 eV full widths at half-maximum.

DOI:10.1063/1674-0068/cjcp1902036

a Ge atom to edge-cap the Ge−Ge bond of Au_2Ge_4 triangular prism of isomer 4A. The theoretical VDE of isomer 5A (2.10 eV) agrees well with the experimental peak at 2.16 eV and that of isomer 5B (3.53 eV) is consistent with the experimental peak at 3.46 eV. The DOS spectrum of isomer 5A can duplicate most of experimental spectral features. Isomer 5C can be ruled out because its theoretical VDE (2.44 eV) is much deviated from the experimental one. Isomer 5D is higher in energy than isomer 5A by 0.14 eV. Therefore, isomer 5A is the most likely one contributing to the photoelectron spectrum of $Au_2Ge_5^-$ and the existence of isomer 5B cannot be excluded.

F. $Au_2Ge_6^-$

In the global minimum (6A) of $Au_2Ge_6^-$, the two Au atoms and six Ge atoms constitute a C_{2v} symmetric tetragonal prism with the two Au atoms located on the top four-membered ring and having a distance of 3.26 Å. The theoretical VDE of isomer 6A (2.26 eV) is in reasonable agreement with the experimental value (2.38 eV) and its DOS spectrum can fit the experimental features very well. Isomers 6B, 6C, and 6D are higher in energy than isomer 6A by 0.15, 0.19, and 0.23 eV, respectively. Therefore, we suggest isomer 6A to be the most probable one observed in the experiments.

G. $Au_2Ge_7^-$

The lowest-lying isomer (7A) of $Au_2Ge_7^-$ can be obtained by adding an additional Ge atom to face-cap the $AuGe_3$ four-membered ring of Au_2Ge_6 tetragonal prism. Isomer 7B can be viewed as an Au atom edge-capping the Ge−Ge bond of Ge_7 pentagonal bipyramid and then another Au atom bonds with the edge-capping Au atom. The theoretical VDEs of isomers 7A and 7B (2.64 and 2.91 eV) are both in line with the experimental value (2.82 eV) and their combined DOS spectrum can roughly duplicate the peak positions, patterns, and intensities of the experimental spectrum. Isomer 7B is slightly higher in energy than isomer 7A by 0.10 eV. The existence of isomers 7C and 7D can be excluded because they are higher in energy than isomer 7A by at least 0.30 eV. Thus, isomer 7A is suggested to be the major one existing in the experiments and the contribution of isomer 7B to the photoelectron spectrum of $Au_2Ge_7^-$ cannot be ruled out.

H. $Au_2Ge_8^-$

In the most stable isomer (8A) of $Au_2Ge_8^-$, a distorted pentagon is composed of two Au atoms and three Ge atoms with the two Au atoms having a distance of 3.40 Å, and then another Ge_5 pentagon interacts with the Au_2Ge_3 pentagon to form a deformable pentagonal prismatic structure. The theoretical VDE of isomer 8A (2.65 eV) is close to the experimental value (2.85 eV) and its DOS spectrum is similar to the experimental one. Isomer 8B is impossible to be detected in the experiments because its theoretical VDE (2.21 eV) is much smaller than the experimental value, although it is higher in energy than isomer 8A by only 0.08 eV. Isomers 8C and 8D are higher in energy than isomer 8A by 0.10 and 0.19 eV, respectively. Hence, isomer 8A is considered as the most probable one detected in the experiments.

I. Au_2Ge_n (n=1−8) neutrals

To explore the charge effect on the geometric structures of Au−Ge mixed clusters, Au_2Ge_{1-8} neutrals were also optimized at the B3LYP level and the results are shown in FIG. 4. The bond lengths of the most stable isomers of Au_2Ge_n (n=1−8) clusters are shown in Table II. We found that the most stable isomers of Au_2Ge_n neutrals have similar structural characteristics to their corresponding anions, except for Au_2Ge_4 and Au_2Ge_5. As for $Au_2Ge_{1-3,6-8}^{-/0}$, the bond lengths and bond angles are different, although their structures are analogous. For example, the ∠AuGeAu angle in Au_2Ge_1 (92.2°) is slightly smaller than that in $Au_2Ge_1^-$ (94.0°), and the ∠AuGeAu angle in Au_2Ge_2 (79.6°) is much smaller than that in $Au_2Ge_2^-$ (104.4°). The lowest-lying isomer of Au_2Ge_4 can be viewed as two additional Au atoms face-capping the Ge_4 rhombic from the opposite directions, similar to the second isomer of $Au_2Ge_4^-$. The ground structure of Au_2Ge_5 can be described as a AuGeAu bent unit above the Ge_4 rhombus.

V. DISCUSSION

We found that the two Au atoms in $Au_2Ge_{1-8}^{-/0}$ tend to occupy high coordination sites and to form more Au−Ge bonds, more likely due to the relative bond strengths between Au−Ge, Ge−Ge, and Au−Au bonds. The bond lengths of Au−Ge (2.46 Å) and Ge−Ge (2.44 Å) are close, but the Au−Ge bond strength (2.84 eV) is stronger than Ge−Ge bond strength (2.78 eV) and Au−Au bond strength (2.35 eV) [101–103], suggesting that the Ge atom prefers to bond with the Au atom rather than other Ge atoms and the Au atom is also inclined to interact with the Ge atom. In other words, the formation of Au−Ge bonds can enhance stability of Au−Ge mixed clusters in comparison to Ge−Ge bonds. These have also been revealed in our previous work of $AuGe_{2-12}^{-/0}$ [63]. In this work, the experimental data suggest that the VDEs of $Au_2Ge_n^-$ gradually increase with the increasing number of Ge atoms. This may relate to the increase of strong Au−Ge bonds from $Au_2Ge_1^-$ to $Au_2Ge_8^-$.

As shown in Table II, the distances between the two Au atoms in $Au_2Ge_{1-8}^{-/0}$ are in the range of 3.21−3.58 Å, both longer than the Au−Au bond length (2.47 Å) in Au_2 dimer [104] and the nearest neighbor

DOI:10.1063/1674-0068/cjcp1902036

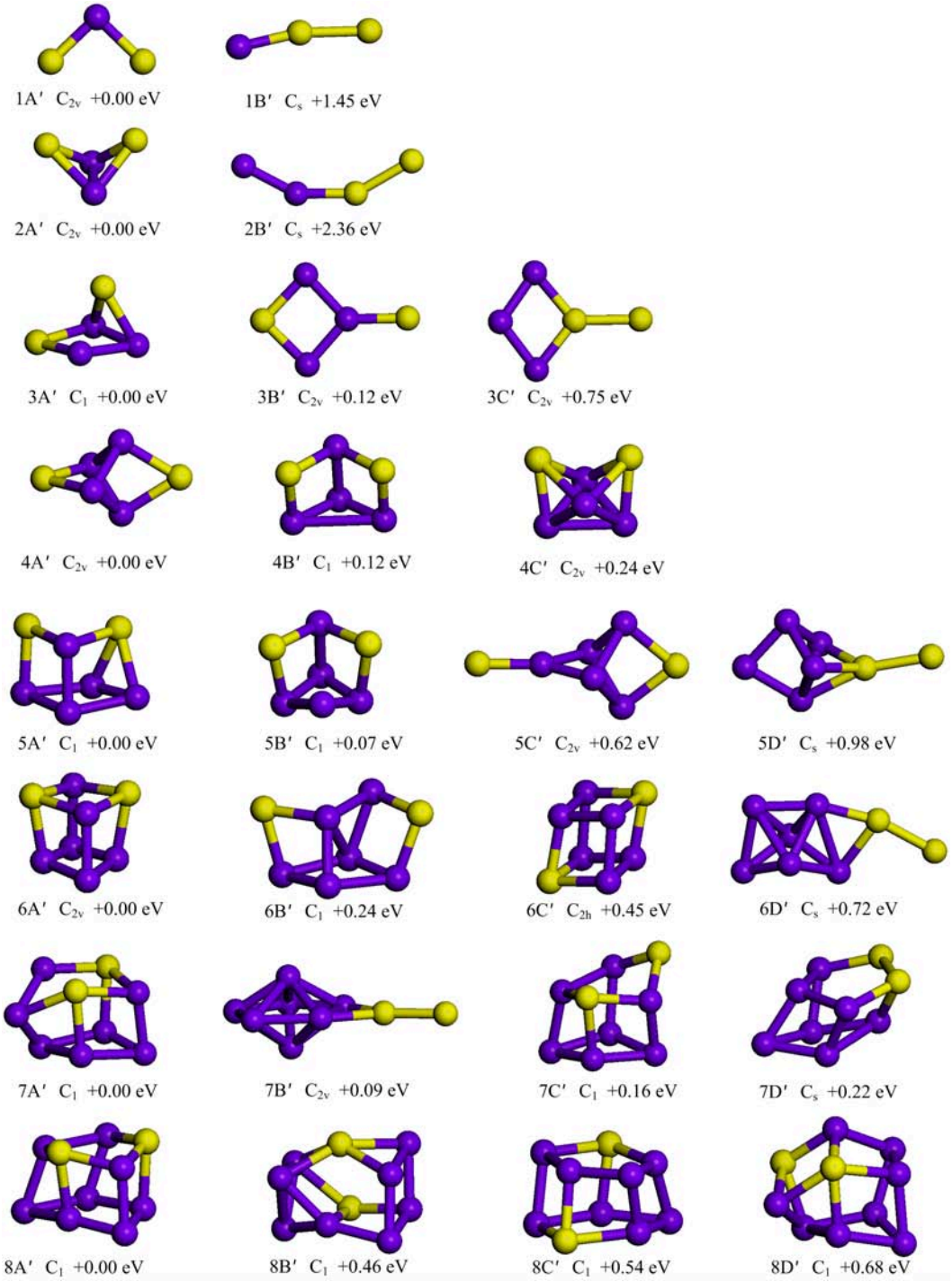

FIG. 4 Typical low-lying isomers of neutral Au_2Ge_n (n=1−8) clusters. Yellow and purple balls stand for the Au atoms and Ge atoms, respectively. ΔE values are calculated at CCSD(T)/aug-cc-pVTZ-PP/Au/aug-cc-pVDZ/Ge level of theory.

distance (2.88 Å) in metallic gold [105], indicating the two Au atoms have weak aurophilic interactions [47]. This is consistent with the relatively weak Au−Au bond strength (2.35 eV) in comparison with Au−Ge bond strength (2.84 eV). However, the previous investigations of $Fe_2Ge_{3-12}{}^{-/0}$ and $Cr_2Ge_{3-14}{}^{-}$ clusters found that the two Fe or Cr atoms incline to bond with each other and to form a strong metal-metal bond [31, 106] suggesting that the bonding properties of $Au_2Ge_n{}^{-/0}$ are different from those of $Fe_2Ge_n{}^{-/0}$ and $Cr_2Ge_n{}^{-}$.

Here, we would like to compare the photoelectron spectra and geometrical structures of $Au_2Ge_{1-7}{}^{-}$ with those of $Au_2Si_{1-7}{}^{-}$ which have been reported in our previous work [71]. The experimental spectra of

DOI:10.1063/1674-0068/cjcp1902036

$Au_2Ge_{1-7}^-$ are rather similar to those of $Au_2Si_{1-7}^-$ except that the experimental VDEs of $Au_2Ge_{1-7}^-$ are slightly higher than those of $Au_2Si_{1-7}^-$. Given that Ge atom has analogical electronic structure with Si atom, it is not surprising to find the similarities of experimental spectra between $Au_2Ge_{1-7}^-$ and $Au_2Si_{1-7}^-$. It is also observed that the two Au atoms in both $Au_2Ge_{1-7}^-$ and $Au_2Si_{1-7}^{-/0}$ have weak aurophilic interactions. As for n=1−6, $Au_2Ge_n^-$ and $Au_2Si_n^-$ adopt analogical geometrical features, which are primarily dominated by the planar ring-like and prismatic based geometries. $Au_2Ge_7^-$ and $Au_2Si_7^-$ have different structural features, in which $Au_2Ge_7^-$ is a Ge-capped Au_2Ge_6 tetragonal prism, while $Au_2Si_7^-$ is a deformable prismatic structure composed of a distorted Au_2Si_3 pentagon and an Si_4 rhombus.

To give insight into the effective atomic charges distribution of $Au_2Ge_{1-8}^-$, we conducted the natural population analysis (NPA) on the most stable isomers and the results are shown in FIG. 5. Since the Pauling electronegativity (χ=2.54) of Au atom is stronger than that (χ=2.01) of Ge atom [107], the negative NPA charges on the two Au atoms in $Au_2Ge_{1-8}^-$ varying from −0.10 e to −0.33 e are expected. The change of NPA charges on the two Au atoms versus n is not significant for $Au_2Ge_{1-8}^-$ because they all adopt exohedral structures. In addition, we found that the NPA charges on the two Au atoms gradually decrease for the cluster sizes of n=1−5 and increase at n=6−8, probably associated with forming more Au−Ge bonds at n=6−8, as a consequence, more electrons of the Ge_n frameworks are transferred to the two Au atoms. The observed increase of VDEs for $Au_2Ge_{1-5}^-$ with the increasing number of Ge atoms may partly be explained by the decrease of the negative NPA charges on the localized Au site. In $Au_2Ge_{1-8}^-$, the two Au atoms interact with nearly same number of Ge atoms, probably resulting in that the NPA charges distribution on the two Au atoms are very similar. Therefore, the NPA charges distribution on the two Au atoms are related with the Pauling electronegativities of Au and Ge atoms and the structural evolution of $Au_2Ge_n^-$ clusters. The charges distribution of Au_2Ge_{1-8} neutrals were also analyzed and were found that the two Au atoms also have a small quantity of negative NPA charges within the range of −(0.01−0.16 e). The Au_2Ge_{1-8} neutrals all have closed-shell electronic structures, as a result, it should be reasonable to find the large HOMO−LUMO gaps. The calculated results suggested that the HOMO−LUMO gaps of Au_2Ge_{1-8} neutrals are between 1.90 and 3.01 eV.

To probe the bonding properties of Au_2Ge_n, we analyzed the molecular orbitals of the most stable isomer of Au_2Ge_6 ($6A'$, $^1A_1$) because it has higher symmetry than the clusters of neighboring sizes as shown in FIG. 6. The HOMO is a σ orbital with bonding characters in the perpendicular Ge−Ge bonds, mainly composed of the $4p_z$ orbitals of four Ge atoms. The

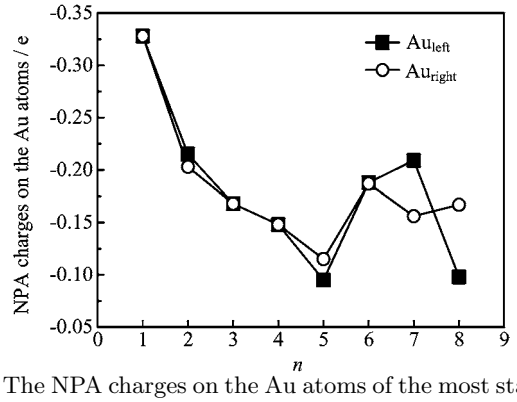

FIG. 5 The NPA charges on the Au atoms of the most stable isomers of $Au_2Ge_n^-$ (n=1−8) clusters.

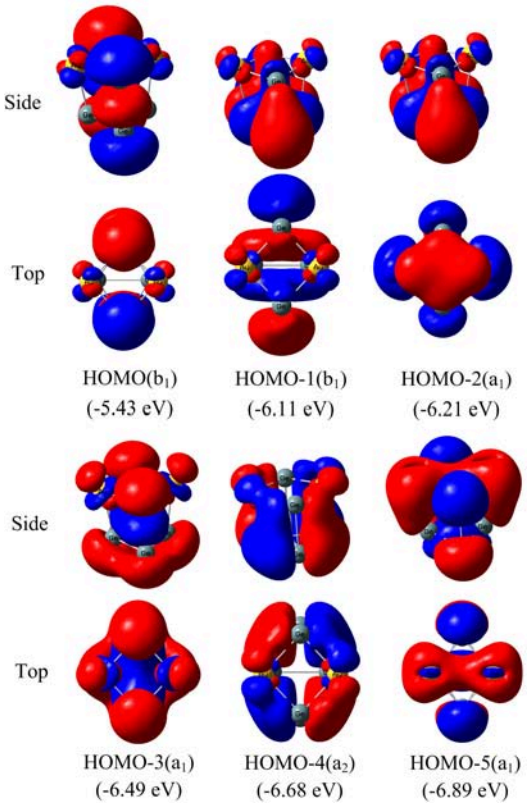

FIG. 6 Molecular orbitals of the lowest-lying isomer ($6A'$, $^1A_1$) of neutral Au_2Ge_6 from different angles (isosurface value=0.02). The alphabet and number in brackets refer to the symmetry of molecular orbitals.

HOMO−1 is a delocalized π orbital with bonding characters in the vertical Au−Ge and Ge−Ge bonds, and HOMO−1 is also a σ orbital with bonding characters in the perpendicular Ge−Ge bonds, primarily constructed by the $5d_{xy}$ orbitals of two Au atoms and the $4p_z$ orbitals of six Ge atoms. The $5d_{z^2}$ orbitals of two Au atoms and the $4p_y$ and $4p_z$ orbitals of six Ge atoms are mainly involved in the HOMO−2, which is a σ orbital with bonding characters in the horizontal Au−Ge and Ge−Ge bonds. The HOMO−3 is a σ orbital with bond-

DOI:10.1063/1674-0068/cjcp1902036

ing characters in the horizontal Ge−Ge bonds, mainly made up of the $5d_{yz}$ orbitals of two Au atoms and the 4s, $4p_x$ and $4p_z$ orbitals of six Ge atoms, whereas the HOMO−4 possesses σ bonding characters and π antibonding characters and has the components from the $5d_{xz}$ orbitals of two Au atoms and the $4p_x$ and $4p_y$ orbitals of six Ge atoms. As for the HOMO−5, it consists of 6s orbitals of two Au atoms and the 4s4p hybridized orbitals of Ge atoms and is a σ orbital with bonding characters. These molecular orbitals clearly suggest that Au_2Ge_6 exhibits σ and π double bonding characters in the vertical Au−Au and Ge−Ge bonds. On one hand, we can see from these MOs that there are small overlaps between the 5d or 6s orbitals of two Au atoms, indicating that the Au−Au interactions are very weak, in reasonable agreement with the long Au−Au distance (3.58 Å) and low Au−Au Wiberg bond order (0.51). On the other hand, there are large overlaps between the 5d or 6s orbitals of two Au atoms and the 4s or 4p orbitals of six Ge atoms, suggesting that the Au−Ge has strong interactions, consistent with high calculated Wiberg bond order of 0.92−0.96. Therefore, the weak Au−Au and strong Au−Ge interactions, and the σ plus π double bonding characters play important roles in the structural stability of C_{2v} symmetric tetragonal prism.

Density of states (DOS) represents the number of states in contiguous unit energy interval and is one of important concepts in solid physics. DOS graph has been considered as a very valuable tool for analyzing the nature of electronic structure, and the curve map of broadened partial density of states (PDOS) can be used for visualizing orbital composition analysis. The Au−Ge and Au−Au interactions can also be interpreted based on the PDOS of the most stable isomer of Au_2Ge_6 ($6A'$, $^1A_1$), as presented in FIG. 7. The p states of Ge and d states of Au are analyzed, and the s states are not given because of its negligible contributions. It can be seen that, for the Au−Ge interactions, there are strong overlaps between Au_2-d and Ge_6-p at energies from −0.2 eV to −1.8 eV and from −3.8 eV to −5.0 eV. For the two Au atoms, it exhibits very weak overlaps between Au_{left}-d and Au_{right}-d. The large overlaps between Au_2-d and Ge_6-p states can confirm the MO analyses that there exit strong interactions between the Au 5d orbitals and the Ge 4p orbitals. The small overlaps between Au_{left}-d and Au_{right}-d states indicate that the Au−Au interactions are weak. This is also consistent with the MO, bond length, and bond order analyses.

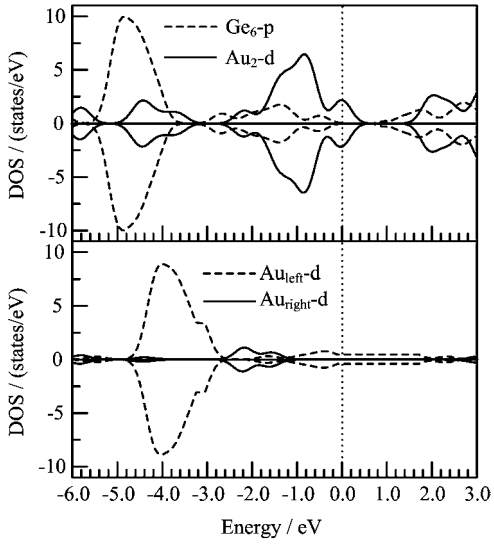

FIG. 7 Partial density of states (PDOS) for the lowest-lying isomer ($6A'$, $^1A_1$) of neutral Au_2Ge_6. The vertical dashed line is the Fermi level.

VI. CONCLUSION

$Au_2Ge_n^{-/0}$ (n=1−8) clusters were investigated by size-selected anion photoelectron spectroscopy and theoretical calculations to probe their structural evolution and electronic properties. The results found that the two Au atoms in $Au_2Ge_n^{-/0}$ (n=1−8) have weak aurophilic interactions and prefer to occupy high coordination sites to form more Au−Ge bonds. The most stable isomers of $Au_2Ge_n^-$ anions and Au_2Ge_n neutrals have spin doublet and singlet states, respectively. It is observed that the most stable structures of $Au_2Ge_n^-$ anions and Au_2Ge_n neutrals adopt similar geometrical characteristics. $Au_2Ge_1^{-/0}$ has a C_{2v} symmetric V-shaped structure, $Au_2Ge_2^{-/0}$ has a C_{2v} symmetric dibridged structure, and $Au_2Ge_3^{-/0}$ can be regarded as the two Au atoms independently capping the different Ge−Ge bonds of Ge_3 triangular structure. $Au_2Ge_{4-8}^{-/0}$ are majorly governed by triangular, tetragonal, and pentagonal prism-based geometries. Especially, Au_2Ge_6 adopts a C_{2v} symmetric tetragonal prism and exihibits σ plus π double bonding characters.

Supplementary materials: The Cartesian coordinates of the low-lying isomers of $Au_2Ge_n^{-/0}$ (n=1−8) clusters are available.

VII. ACKNOWLEDGEMENTS

This work was supported by the National Natural Science Foundation of China (No.21273246 and No.21103202), the Chinese Academy of Sciences (No.QYZDB-SSW-SLH024), the Natural Science Foundation of Shandong Province of China (No.ZR2018BB040), Open Funds of Beijing National Laboratory for Molecular Sciences (No.BNLMS201804), Research Start-up Funds (Doctoral Science Foundation) of Heze University (No.XY18BS02), and Chinese Academy of Sciences President's International Fellowship Initiative (PIFI) (No.2018VMA0011). The theoretical calculations are performed on the China Scientific Computing Grid (ScGrid) of the Supercomputing Center, Computer

Network Information Center of the Chinese Academy of Sciences.

[1] Y. Kamata, Mater. Today **11**, 30 (2008).
[2] R. Pillarisetty, Nature **479**, 324 (2011).
[3] M. Amato, M. Palummo, R. Rurali, and S. Ossicini, Chem. Rev. **114**, 1371 (2014).
[4] Z. Luo and A. W. Castleman, Acc. Chem. Res. **47**, 2931 (2014).
[5] T. Zhao, Q. Wang, and P. Jena, ACS Energy Lett. **1**, 202 (2016).
[6] P. Jena and Q. Sun, Chem. Rev. **118**, 5755 (2018).
[7] G. R. Burton, C. Xu, C. C. Arnold, and D. M. Neumark, J. Chem. Phys. **104**, 2757 (1996).
[8] Y. Negishi, H. Kawamata, H. T, M. Gomei, R. Kishi, F. Hayakawa, A. Nakajima, and K. Kaya, Chem. Phys. Lett. **269**, 199 (1997).
[9] M. Scheer, R. Bilodeau, C. A. Brodie, and H. K. Haugen, Phys. Rev. A **58**, 2844 (1998).
[10] Z. Y. Lu, C. Z. Wang, and K. M. Ho, Phys. Rev. B **61**, 2329 (2000).
[11] B. X. Li and P. L. Cao, Phys. Rev. B **62**, 15788 (2000).
[12] J. Wang, G. Wang, and J. Zhao, Phys. Rev. B **64**, 205411 (2001).
[13] L. Z. Zhao, W. C. Lu, W. Qin, Q. J. Zang, C. Z. Wang, and K. M. Ho, Chem. Phys. Lett. **455**, 225 (2008).
[14] D. Bandyopadhyay and P. Sen, J. Phys. Chem. A **114**, 1835 (2010).
[15] S. Bals, S. V. Aert, C. P. Romero, K. Lauwaet, M. J. V. Bael, B. Schoeters, B. Partoens, E. Ycelen, P. Lievens, and G. V. Tendeloo, Nat. Commun. **3**, 897 (2012).
[16] W. An, Phys. Chem. Chem. Phys. **20**, 25746 (2018).
[17] D. Wu, R. Shi, Q. Du, X. Wu, X. Liang, X. Huang, L. Sai, and J. Zhao, J. Clust. Sci. **30**, 371 (2019).
[18] L. Wang and J. Zhao, J. Chem. Phys. **128**, 024302 (2008).
[19] X. Zhang, G. Li, and Z. Gao, Rapid Commun. Mass Spectrom. **15**, 1573 (2001).
[20] J. Lu and S. Nagase, Chem. Phys. Lett. **372**, 394 (2003).
[21] J. Wang and J. G. Han, J. Chem. Phys. **123**, 244303 (2005).
[22] J. Wang and J. G. Han, J. Phys. Chem. B **110**, 7820 (2006).
[23] J. Wang and J. G. Han, J. Phys. Chem. A **46**, 12670 (2006).
[24] J. Wang and J. G. Han, Chem. Phys. **342**, 253 (2007).
[25] Q. Jing, F. Y. Tian, and Y. X. Wang, J. Chem. Phys. **128**, 124319 (2008).
[26] J. Wang and J. G. Han, J. Phys. Chem. A **112**, 3224 (2008).
[27] W. J. Zhao and Y. X. Wang, Chem. Phys. **352**, 291 (2008).
[28] S. Furuse, K. Koyasu, J. Atobe, and A. Nakajima, J. Chem. Phys. **129**, 064311 (2008).
[29] W. J. Zhao and Y. X. Wang, J. Mol. Struct.: THEOCHEM. **901**, 18 (2009).
[30] X. J. Deng, X. Y. Kong, X. Liang, B. Yang, H. G. Xu, X. L. Xu, G. Feng, and W. J. Zheng, J. Chem. Phys. **147**, 234310 (2017).
[31] X. Liang, X. Kong, S. J. Lu, Y. Huang, J. Zhao, H. G. Xu, W. Zheng, and X. C. Zeng, J. Phys.: Condens. Matter **30**, 335501 (2018).
[32] X. J. Deng, X. Y. Kong, X. L. Xu, H. G. Xu, and W. J. Zheng, ChemPhysChem **15**, 3987 (2014).
[33] X. J. Deng, X. Y. Kong, X. Liang, B. Yang, H. G. Xu, X. L. Xu, G. Feng, and W. J. Zheng, J. Chem. Phys. **147**, 234310 (2017).
[34] X. J. Deng, X. Y. Kong, H. G. Xu, X. L. Xu, G. Feng, and W. J. Zheng, J. Phys. Chem. C **119**, 11048 (2015).
[35] X. J. Deng, X. Y. Kong, X. L. Xu, H. G. Xu, and W. J. Zheng, RSC Adv. **4**, 25963 (2014).
[36] X. J. Deng, X. Y. Kong, X. L. Xu, H. G. Xu, and W. J. Zheng, Chin. J. Chem. Phys. **29**, 123 (2016).
[37] A. Fert, V. Cros, and J. Sampaio, Nat. Nanotechnol. **8**, 152 (2013).
[38] V. Franco, J. S. Blazquez, B. Ingale, and A. Conde, Annu. Rev. Mater. Res. **42**, 305 (2012).
[39] F. Albertini, D. Negri, L. Pareti, E. B. Watts, Z. Arnold, J. Kamarad, G. Calestani, A. Deriu, and S. Besseghin, J. Appl. Phys. **96**, 2110 (2004).
[40] A. Brataas, A. D. Kent, and H. Ohno, Nat. Mater. **11**, 372 (2012).
[41] X. Z. Yu, N. Kanazawa, Y. Onose, K. Kimoto, W. Z. Zhang, S. Ishiwata, Y. Matsui, and Y. Tokura, Nat. Mater. **10**, 106 (2011).
[42] Y. Jin, G. Maroulis, X. Kuang, L. Ding, C. Lu, J. Wang, J. Lv, C. Zhang, and M. Ju, Phys. Chem. Chem. Phys. **17**, 13590 (2015).
[43] Y. Jin, Y. Tian, X. Kuang, C. Zhang, C. Lu, J. Wang, J. Lv, L. Ding, and M. Ju, J. Phys. Chem. A **119**, 6738 (2015).
[44] X. X. Xia, A. Hermann, X. Y. Kuang, Y. Y. Jin, C. Lu, and X. D. Xing, J. Phys. Chem. C **120**, 677 (2016).
[45] W. G. Sun, J. J. Wang, C. Lu, X. X. Xia, X. Y. Kuang, and A. Hermann, Inorg. Chem. **56**, 1241 (2017).
[46] P. Pyykkö, Chem. Rev. **88**, 563 (1988).
[47] P. Pyykkö, Angew. Chem. Int. Ed. **43**, 4412 (2004).
[48] J. P. Desclaux and P. Pyykkö, Chem. Phys. Lett. **39**, 300 (1976).
[49] J. Lin, S. Zhang, W. Guan, G. Yang, and Y. Ma, J. Am. Chem. Soc. **140**, 9545 (2018).
[50] B. Kiran, X. Li, H. J. Zhai, L. F. Cui, and L. S. Wang, Angew. Chem. Int. Ed. **43**, 2125 (2004).
[51] R. A. Wood, J. Appl. Phys. **36**, 1490 (1965).
[52] T. M. Berlicki, E. Murawski, M. Muszynski, S. J. Osadnik, and E. L. Prociow, Sensor. Actuat. A **50**, 183 (1995).
[53] X. X. Wang, M. Getaneh, C. J. Martoff, and E. Kaczanowicz, J. Appl. Phys. **85**, 8274 (1999).
[54] A. Spiekermann, S. Hoffmann, F. Kraus, and T. F. Fassler, Angew. Chem. Int. Ed. **46**, 1638 (2007).
[55] C. Schenk and A. Schnepf, Angew. Chem. Int. Ed. **46**, 5314 (2007).
[56] M. E. Dávila, L. Xian, S. Cahangirov, A. Rubio, and G. Le Lay, New J. Phys. **16**, 095002 (2014).
[57] X. J. Li and K. H. Su, Theor. Chem. Acc. **124**, 345 (2009).
[58] B. T. Truong and M. T. Nguyen, J. Phys. Chem. A **115**, 9993 (2011).
[59] X. J. Li, H. J. Ren, and L. M. Yang, J. Nanomater. **2012**, 1 (2012).

DOI:10.1063/1674-0068/cjcp1902036

[60] X. Li, K. Su, X. Yang, L. Song, and L. Yang, J. Comput. Chem. **1010**, 32 (2013).
[61] J. M. Goicoechea and J. E. McGrady, Dalton Trans. **44**, 6755 (2015).
[62] D. McDermott and K. E. Newman, Eur. Phys. J. D **69**, 90 (2015).
[63] S. J. Lu, L. R. Hu, X. L. Xu, H. G. Xu, H. Chen, and W. J. Zheng, Phys. Chem. Chem. Phys. **18**, 20321 (2016).
[64] Q. T. Tran, S. J. Lu, L. J. Zhao, X. L. Xu, H. G. Xu, V. T. Tran, J. Li, and W. J. Zheng, J. Phys. Chem. A **122**, 3374 (2018).
[65] H. G. Xu, Z. G. Zhang, Y. Feng, J. Yuan, Y. Zhao, and W. Zheng, Chem. Phys. Lett. **487**, 204 (2010).
[66] G. W. T. M. J. Frisch, H. B. Schlegel, G. E. Scuseria, M. A. Robb, J. R. Cheeseman, G. Scalmani, V. Barone, G. A. Petersson, H. Nakatsuji, X. Li, M. Caricato, A. Marenich, J. Bloino, B. G. Janesko, R. Gomperts, B. Mennucci, H. P. Hratchian, J. V. Ortiz, A. F. Izmaylov, J. L. Sonnenberg, D. Williams-Young, F. Ding, F. Lipparini, F. Egidi, J. Goings, B. Peng, A. Petrone, T. Henderson, D. Ranasinghe, V. G. Zakrzewski, J. Gao, N. Rega, G. Zheng, W. Liang, M. Hada, M. Ehara, K. Toyota, R. Fukuda, J. Hasegawa, M. Ishida, T. Nakajima, Y. Honda, O. Kitao, H. Nakai, T. Vreven, K. Throssell, J. A. Montgomery, Jr., J. E. Peralta, F. Ogliaro, M. Bearpark, J. J. Heyd, E. Brothers, K. N. Kudin, V. N. Staroverov, T. Keith, R. Kobayashi, J. Normand, K. Raghavachari, A. Rendell, J. C. Burant, S. S. Iyengar, J. Tomasi, M. Cossi, J. M. Millam, M. Klene, C. Adamo, R. Cammi, J. W. Ochterski, R. L. Martin, K. Morokuma, O. Farkas, J. B. Foresman, and D. J. Fox, *Gaussian 09, Revision A.02*, Wallingford CT: Gaussian, Inc. (2009).
[67] J. Lv, Y. C. Wang, L. Zhu, and Y. M. Ma, J. Chem. Phys. **137**, 084104 (2012).
[68] S. J. Lu, H. G. Xu, X. L. Xu, and W. J. Zheng, J. Phys. Chem. C **121**, 11851 (2017).
[69] S. J. Lu, L. S. Wu, and F. Lin, Chem. Phys. Lett. **707**, 108 (2018).
[70] S. J. Lu, L. S. Wu, and F. Lin, Comput. Theor. Chem. **1139**, 102 (2018).
[71] S. J. Lu, X. L. Xu, H. G. Xu, and W. J. Zheng, J. Chem. Phys. **148**, 244306 (2018).
[72] S. J. Lu, L. S. Wu, and F. Lin, Chem. Phys. Lett **709**, 60 (2018).
[73] S. J. Lu, X. L. Xu, G. J. Cao, H. G. Xu, and W. J. Zheng, J. Phys. Chem. C **122**, 2391 (2018).
[74] S. J. Lu, X. L. Xu, G. Feng, H. G. Xu, and W. J. Zheng, J. Phys. Chem. C **120**, 25628 (2016).
[75] A. D. Becke, J. Chem. Phys. **98**, 1372 (1993).
[76] A. D. Becke, J. Chem. Phys. **98**, 5648 (1993).
[77] C. Lee, W. Yang, and R. G. Parr, Phys. Rev. B: Condens. Matter Mater. Phys. **37**, 785 (1988).
[78] P. J. Stephens, F. J. Devlin, C. F. Chabalowski, and M. J. Frisch, J. Phys. Chem. **98**, 11623 (1994).
[79] V. Rassolov, J. A. Pople, M. Ratner, and T. L. Windus, J. Chem. Phys. **109**, 1223 (1998).
[80] P. J. Hay and W. R. Wadt, J. Chem. Phys. **82**, 299 (1985).
[81] J. P. Blaudeau, M. P. McGrath, L. A. Curtiss, and L. Radom, J. Chem. Phys. **107**, 5016 (1997).
[82] M. Dolg, U. Wedig, H. Stoll, and H. Preuss, J. Chem. Phys. **86**, 866 (1987).
[83] G. D. Purvis and R. J. Bartlett, J. Chem. Phys. **76**, 1910 (1982).
[84] G. E. Scuseria and H. F. Schaefer, J. Chem. Phys. **90**, 3700 (1989).
[85] K. A. Peterson, D. Figgen, M. Dolg, and H. Stoll, J. Chem. Phys. **126**, 124101 (2007).
[86] K. A. Peterson, J. Chem. Phys. **119**, 11099 (2003).
[87] R. Naaman and Z. Vager, *In the Structure of Small Molecules and Ions*, New York: Plenum Press, 1115 (1988).
[88] J. P. Foster and F. Weinhold, J. Am. Chem. Soc. **102**, 7211 (1980).
[89] A. E. Reed and F. Weinhold, J. Chem. Phys. **78**, 4066 (1983).
[90] A. E. Reed, R. B. Weinstock, and F. Weinhold, J. Chem. Phys. **83**, 735 (1985).
[91] A. E. Reed and F. Weinhold, J. Chem. Phys. **83**, 1736 (1985).
[92] J. E. Carpenter, *PhD. Thesis*, University of Wisconsin, (1987).
[93] J. E. Carpenter and F. Weinhold, J. Mol. Struct.: THEOCHEM **169**, 41 (1988).
[94] A. E. Reed, L. A. Curtiss, and F. Weinhold, Chem. Rev. **88**, 899 (1988).
[95] T. Lu and F. Chen, J. Comput. Chem. **33**, 580 (2012).
[96] E. D. Glendening, C. R. Landis, and F. Weinhold, WIREs Comput. Mol. Sci. **2**, 1 (2012).
[97] A. E. Reed and F. Weinhold, J. Chem. Phys. **83**, 1736 (1985).
[98] J. Akola, M. Manninen, H. Hakkinen, U. Landman, X. Li, and L. S. Wang, Phys. Rev. B: Condens. Matter Mater. Phys. **60**, 297 (1999).
[99] D. J. Tozer and N. C. Handy, J. Chem. Phys. **109**, 10180 (1998).
[100] S. J. Lu, X. L. Xu, G. J. Cao, H. G. Xu, and W. J. Zheng, J. Chem. Phys. **149**, 174314 (2018).
[101] A. Neckel and G. Sodeck, Monatsh. Chem. **103**, 367 (1972).
[102] I. Shima, M. S. Babab, and K. A. Gingerichb, Chem. Phys. **277**, 9 (2002).
[103] B. M. Smirnov and A. S. Yatsenko, Physics-Uspekhi **39**, 211 (1996).
[104] B. Simard and P. A. Hackett, J. Mol. Spectrosc. **142**, 310 (1990).
[105] R. W. G. Wyckoff, *Crystal Structures*, New York: Interscience (1963).
[106] X. Q. Liang, X. J. Deng, S. J. Lu, X. M. Huang, J. J. Zhao, H. G. Xu, W. J. Zheng, and X. C. Zeng, J. Phys. Chem. C **121**, 7037 (2017).
[107] L. Pauling, J. Am. Chem. Soc. **54**, 3570 (1932).

DOI:10.1063/1674-0068/cjcp1902036